Eur. Phys. J. C (2021) 81:1027
https://doi.org/10.1140/epjc/s10052-021-09818-x

THE EUROPEAN PHYSICAL JOURNAL C

Regular Article - Theoretical Physics

Analytical external spherical solutions in entangled relativity

Denis Arruga, Olivier Minazzoli[a]

Artemis, Université Côte d'Azur, CNRS, Observatoire Côte d'Azur, BP 4229, 06304 Nice Cedex 4, France

Received: 28 September 2021 / Accepted: 6 November 2021 / Published online: 24 November 2021

Abstract In this manuscript, we present analytical external spherical solutions of entangled relativity, which we compare to numerical solutions obtained in a Tolman–Oppenheimer–Volkoff framework. Analytical and numerical solutions match perfectly well outside spherical compact objects, therefore validating both types of solutions at the same time. The analytical external (hairy) solutions – which depend on two parameters only – may be used in order to easily compute observables – such as X-ray pulse profiles – without having to rely on an unknown equation of state for matter inside the compact object.

1 Introduction

Entangled relativity is a new general theory of relativity that changes the way spacetime and matter interact with each other [2,22,25].[1] Instead of assuming that the spacetime and matter parts of the action have to be glued together additively, it is assumed in entangled relativity that they are glued together multiplicatively instead. This has the immediate consequence that gravity and inertia cannot be defined without defining matter at the same time, and vice-versa – therefore satisfying Einstein's main version of Mach's Principle [10][2] and [35].

While the pure multiplicative coupling in the action could (naïvely) question the viability of the theory, it turns out that the action can be written in a form of a scalar–tensor theory that possesses an *intrinsic decoupling* of the scalar-field degree of freedom [22,25]. This means that the theory possesses the same degrees of freedom as a scalar–tensor theory – therefore ensuring its theoretical viability – and that the scalar-field is not, or weakly, sourced in most situations, such that the phenomenology of entangled relativity is very close to the one of general relativity in many cases [2,24,26,28,29,31].

Recently, we studied numerical solutions of compact objects in entangled relativity [2]. Here, we present analytical external solutions for spherical objects, which we then compare to our numerical solutions. We find that the analytical and numerical solutions match with each other, providing evidence of the validity of each of them. Since the analytical solutions depend on two parameters only, they may be useful in order to easily compute observables related to neutron stars – such as X-ray pulse profiles [6,23,36]; whereas numerical solutions could then be used, in a second time, in order to check what types of equation of state can produce the fitted values of the parameters.

Along the way, we recovered an old analytical solution for spherical objects with scalar hairs that does not seem to be widely known by the community.

2 Field equations

The action of entangled relativity is defined by Minazzoli [25] and Ludwig et al. [22]

$$S = -\frac{\xi}{2}\int \mathrm{d}^4x\sqrt{-g}\frac{\mathcal{L}_m^2}{R}, \tag{1}$$

where the coupling constant ξ has the dimension of $\kappa \equiv 8\pi G/c^4$ – where G is the Newtonian constant and c the speed of light – but not its value. In fact, ξ does not appear in the field equations that derive from the extremization of the action (1), and therefore is purely related to the quantum field sector of the theory. It is important to note that apart from ξ, the theory does not have any coupling constant related to the link between matter and geometry. Hence, at the classical level, entangled relativity has one parameter less than gen-

[a] e-mail: ominazzoli@gmail.com (corresponding author)

[1] The name *entangled relativity* appears for the first time in Arruga et al. [2].

[2] A translation in English of the original paper in German is available online at https://einsteinpapers.press.princeton.edu/vol7-trans/49.

eral relativity in order to describe the link between matter and geometry, in the sense that no parameter replaces the parameter κ of general relativity at the classical level in entangled relativity [25]: the effective coupling that appears at the level of the field equation is dynamical. For $\mathcal{L}_m \neq 0$, the metric field equation reads[3]

$$R_{\mu\nu} - \frac{1}{2} g_{\mu\nu} R = -\frac{R}{\mathcal{L}_m} T_{\mu\nu} + \frac{R^2}{\mathcal{L}_m^2} \left(\nabla_\mu \nabla_\nu - g_{\mu\nu} \Box \right) \frac{\mathcal{L}_m^2}{R^2}, \quad (2)$$

with

$$T_{\mu\nu} \equiv -\frac{2}{\sqrt{-g}} \frac{\delta \left(\sqrt{-g} \mathcal{L}_m \right)}{\delta g^{\mu\nu}}. \quad (3)$$

Also note that the stress–energy tensor is no longer conserved in general, as one has

$$\nabla_\sigma \left(\frac{\mathcal{L}_m}{R} T^{\alpha\sigma} \right) = \mathcal{L}_m \nabla^\alpha \left(\frac{\mathcal{L}_m}{R} \right). \quad (4)$$

Otherwise, note that the trace of Eq. (2) reads

$$3 \frac{R^2}{\mathcal{L}_m^2} \Box \frac{\mathcal{L}_m^2}{R^2} = -\frac{R}{\mathcal{L}_m} \left(T - \mathcal{L}_m \right). \quad (5)$$

The *intrinsic decoupling* of the scalar degree of freedom is manifest for $\mathcal{L}_m = T$ [24–26,28–30]. Indeed, for $\mathcal{L}_m = T$ on-shell – such as for a dust field, or null-radiation – $\mathcal{L}_m/R =$ constant is solution of the trace of the metric field equation (5), such that one recovers the metric field equation of general relativity in that case [25].

It is important to notice that the coupling constant between matter and geometry in the metric field equation of general relativity is replaced by a scalar field degree of freedom in entangled relativity that corresponds to the ratio between R and $\mathcal{L}_m$: $8\pi G_{\text{eff}}/c^4 := -R/\mathcal{L}_m$ [25]. In particular, the effective coupling in the metric field equation of entangled relativity is positive for $\mathcal{L}_m/R < 0$ and negative for $\mathcal{L}_m/R > 0$, potentially providing a repulsive mechanism at high density, where the kinetic energy density should dominate in the on-shell matter Lagrangian [27,32]. [4]

Indeed, as a star collapse into a black hole, the kinetic part K of the matter Lagrangian density shall ineluctably start to dominate the whole Lagrangian density on-shell – that is $K > V$, such that $\mathcal{L}_m := K - V > 0$, where V is the potential part of the Lagrangian density. If, in the meantime, R keeps the same sign, then gravity shall become repulsive and the collapsing matter shall rebound due to the new repulsive nature of gravity. This should avoid the formation of spacetime singularities inside black holes in the framework of entangled relativity.

The avoidance of singularities in entangled relativity is also somewhat expected given that the theory prohibits the existence of spacetime without matter at a fundamental level [22,25,32].

3 Almost equivalent action

At least for spacetimes that are such that $(R, \mathcal{L}_m) \neq 0$, there is a one to two correspondence at the classical level between the action of entangled relativity and a dilaton theory with the following action [22,25]

$$S = \frac{1}{c} \frac{\xi}{\tilde{\kappa}} \int d^4x \sqrt{-g} \left[\frac{\phi R}{2\tilde{\kappa}} + \sqrt{\phi} \mathcal{L}_m \right], \quad (6)$$

where $\tilde{\kappa}$ is an effective coupling constant between matter and geometry, with the dimension of the coupling constant of general relativity κ. Because entangled relativity leads to a repulsive gravitational phenomenon for $\mathcal{L}_m/R > 0$, the action in Eq. (6) corresponds to the original action in Eq. (1) as long as one has $\tilde{\kappa} > 0$ if $\mathcal{L}_m/R < 0$, and $\tilde{\kappa} < 0$ if $\mathcal{L}_m/R > 0$. The corresponding field equations read

$$G_{\alpha\beta} = \tilde{\kappa} \frac{T_{\alpha\beta}}{\sqrt{\phi}} + \frac{1}{\phi} \left[\nabla_\alpha \nabla_\beta - g_{\alpha\beta} \Box \right] \phi, \quad (7)$$

$$\sqrt{\phi} = -\tilde{\kappa} \mathcal{L}_m / R. \quad (8)$$

The conservation equation reads

$$\nabla_\sigma \left(\sqrt{\phi} T^{\alpha\sigma} \right) = \mathcal{L}_m \nabla^\alpha \sqrt{\phi}, \quad (9)$$

The trace of the metric field equation can therefore be rewritten as follows

$$\frac{3}{\phi} \Box \phi = \frac{\tilde{\kappa}}{\sqrt{\phi}} \left(T - \mathcal{L}_m \right). \quad (10)$$

The equivalence between Eqs. (7–10) and (2–4) is pretty straightforward to check.

4 Generic external vacuum solutions in scalar–tensor theories

Let us consider the following generic class of actions[5]

[3] The metric field equation for all $\mathcal{L}_m$ is given in the Appendix A.

[4] While the transition between the attractive and repulsive cases seems to be singular in Eq. (2), it is not the case when one looks at the actual metric field equation for all $\mathcal{L}_m$ given in Eq. (A.1).

[5] For now on, we use the unit system that is such that $G = c = \mu_0 = 1$.

$$S = \int d^4x\sqrt{-g}\left[R - 2(\nabla\varphi)^2 + f(\varphi, \mathcal{L}_m)\right], \tag{11}$$

that is such that one has in the vacuum limit ($\mathcal{L}_m \to 0$)

$$\lim_{\mathcal{L}_m \to 0} f(\varphi, \mathcal{L}_m) \to 0. \tag{12}$$

For instance, Brans–Dick theory in the Einstein frame implies that $f(\varphi, \mathcal{L}_m) = \mathcal{L}_m(A^2(\varphi)g_{\mu\nu})$ [41], whereas low-energy string, supergravity, Kaluza–Klein and entangled relativity theories in the Einstein frame generically imply that $f(\varphi, \mathcal{L}_m) = f(\varphi)\mathcal{L}_m(A^2(\varphi)g_{\mu\nu})$ [8,13,32], while general relativity corresponds to $f(\varphi, \mathcal{L}_m) = \mathcal{L}_m(g_{\mu\nu})$. The action (6) can be put in the form of the action (11) after the conformal transformation of the metric $g_{\alpha\beta} \to e^{-2\varphi/\sqrt{3}}g_{\alpha\beta}$, with $\phi = e^{-2\varphi/\sqrt{3}}$ – see Sect. 5.

We found that a class of vacuum spherical solutions for the generic class of actions (11) reads

$$ds^2 = -\left(1 - \frac{2m}{\beta r}\right)^{\beta} \mathrm{d}t^2 + \left(1 - \frac{2m}{\beta r}\right)^{-\beta} \mathrm{d}r^2 + r^2\left(1 - \frac{2m}{\beta r}\right)^{1-\beta}\left[\mathrm{d}\theta^2 + \sin^2\theta\,\mathrm{d}\psi^2\right], \tag{13}$$

with

$$\varphi = \frac{1-\beta}{2\alpha}\ln\left(1 - \frac{2m}{\beta r}\right) \tag{14}$$

where

$$\alpha^2 = \frac{1-\beta}{1+\beta}, \tag{15}$$

where $\beta \in [-1; 0[\cup]0; 1]$ (or equivalently $\alpha \in \mathbb{R} - \{1\}$).[6] One can either have $\alpha \geq 0$ or $\alpha \leq 0$ because the action is invariant under the reflection ($\mathbb{Z}$-2) symmetry $\varphi \to -\varphi$ at the limit $\mathcal{L}_m = 0$. One recovers the usual Schwarzschild metric for $\beta = 1$ (or equivalently $\alpha = 0$).[7] Hence, Eqs. (13–15) are a generalization of the Schwarzschild metric for all the theories that can be written in the form of Eqs. (11–12). The solutions described by the Eqs. (13–15) are also much simpler than the Janis–Newman–Winicour solutions [19] – although they ought to describe the same spacetimes, albeit with different coordinates. After some investigation of the literature, we found that the solutions in Eqs. (13–15) can already be found in Damour and Esposito-Farese [7], and that it has been attributed to Just [21].

It is crucial to understand that Eqs. (13–15) are vacuum solutions of Eqs. (11–12) for all $\beta \in]-1; 0[\cup]0; 1]$. It means that any theory that can be written in the form of Eqs. (11–12), has a family of solutions that reads as Eqs. (13–15), with various values for the parameters m and β. As a consequence, all theories that can be written as Eqs. (11–12) have spherical solutions that do not only depend on a mass, but on the parameter β as well. We shall therefore qualify these solutions as *hairy* ones.

It is therefore quite different from the charged spherical solutions in the Einstein–Maxwell-dilaton theories [12,18], for which a similar parameter α is fixed by the theory that one considers – like for instance $\alpha = 1$ for the tree-level low-energy limit of string theory and ($D = 4$, $N = 4$) supergravity, or $\alpha = \sqrt{3}$ for 5D Kaluza–Klein theory [13], or $\alpha = 1/(2\sqrt{3})$ for entangled relativity [32]. Here, on the other hand, the theory does not constrain the value of α nor β. Indeed, α and β do not appear in the Lagrangian density, unlike in the Einstein–Maxwell-dilaton cases, where α corresponds to the coupling strength between the scalar and electromagnetic fields in the Lagrangian density [12,18].

It is important to note that Eqs. (13–15) are solutions of general relativity as well, provided that there is a massless canonical scalar field – for which, as far as we know, there is currently no evidence for in nature. One might therefore think that the solutions in Eqs. (13–15) violate Birkhoff's theorem [15], but that is not the case. Indeed, the presence of the scalar-field in the action (11) implies that one is not dealing with general relativity in vacuum, while Birkhoff's theorem applies to general relativity in vacuum [15].

It is also important to note that $r = 2m/\beta$ is a curvature singularity for all $\beta \in]0; 1[$ (or equivalently $\alpha \in]0; 1[$) – see Appendix D – whereas it is an event horizon for the Schwarzschild case – that is, for $\beta = 1$ (or equivalently $\alpha = 0$). However, such a singularity is not expected to happen in nature due to the fact that scalar hairs are radiated away during the collapse into a black-hole in scalar–tensor theories of the form of (11–12), leading to black holes with no hair [5,14,16,38,40]. Therefore, while the solutions in Eqs. (13–15) should be exact external solutions of spherical objects, they should not correspond to pure vacuum solutions – unlike the Schwarzschild and Kerr black holes for instance.

Nevertheless, direct observations of the *shadow* of diverse black holes [11,33] – such as the one done with the Event Horizon Telescope for M87 [11] – and the corresponding signatures of photons *subrings* [20], could be used in order to test $\beta \neq 1$ solutions – that is solutions with scalar hairs – for actual astrophysical objects that are currently supposed to be black holes. The goal would be to test the existence of scalar hairs, despite the fact that they are currently not expected at the theoretical level.

[6] We check these solutions in Appendix B.

[7] Actually, one can show that the metric (13) is invariant under the transformation $\beta \to -\beta$, with a shifted radial coordinate ρ as $\rho = r - 2m/\beta$ – see Appendix C.

4.1 Comment on the vacuum limit in entangled relativity

Let us note that entangled relativity corresponds to $f(\varphi, \mathcal{L}_m) = f(\varphi)\mathcal{L}_m(e^{\alpha\varphi} g_{\mu\nu})$ like usual dilaton theories, provided that one has $\mathcal{L}_m \neq 0$ and $R \neq 0$ [2,22,25]. This means that while the solutions (13–15) cannot be exact solutions of entangled relativity, they should be good approximations in the vacuum limit of the theory – that is, when $T_{\mu\nu} \to 0$ but $T_{\mu\nu} \neq 0$ – just as the Schwarzschild metric has been found to be a good approximation of spherical black holes in this limit in Minazzoli and Santos [32].

5 Dilaton action and solutions in the Einstein frame

After the conformal transformation $\tilde{g}_{\alpha\beta} = e^{-2\varphi/\sqrt{3}} g_{\alpha\beta}$, with $\phi = e^{-2\varphi/\sqrt{3}}$, the action (6) reads

$$S = \int d^4x\sqrt{-\tilde{g}}\Big[\tilde{R} - 2\tilde{g}^{\alpha\beta}\partial_\alpha\varphi\partial_\beta\varphi \tag{16}$$

$$+e^{-\varphi/\sqrt{3}}\tilde{\mathcal{L}}_m(e^{2\varphi/\sqrt{3}}\tilde{g}_{\mu\nu})\Big], \tag{17}$$

where $\tilde{\mathcal{L}}_m := e^{4\varphi/\sqrt{3}}\mathcal{L}_m$. It means that it corresponds to

$$f(\varphi, \tilde{\mathcal{L}}_m) = e^{-\varphi/\sqrt{3}}\tilde{\mathcal{L}}_m(e^{2\varphi/\sqrt{3}}\tilde{g}_{\mu\nu}) \tag{18}$$

in Eq. (11), in which one would have $g_{\alpha\beta} := \tilde{g}_{\alpha\beta}$. One can check that $\delta(\sqrt{-\tilde{g}}f)/\delta\varphi = 0\ \forall\ \tilde{\mathcal{L}}_m = \tilde{T}$ – or, equivalently, $\mathcal{L}_m = T$ in the field equations in the original frame – such that the scalar-field equation reduces to $\Box\varphi = 0\ \forall\ \tilde{\mathcal{L}}_m = \tilde{T}$ on-shell. This is the property of what has been called *intrinsic decoupling* in Minazzoli and Hees [28,29]. Note that one notably has $\mathcal{L}_m = T$ for dust and pure electromagnetic radiation for instance; whereas one has $\mathcal{L}_m \neq T$ for an electric or a magnetic field – notably leading to different charged black-holes with respect to the ones of general relativity [32].

One can therefore use the external solutions (13–15), that we shall rewrite as follows (for later convenience):

$$ds^2 = -\left(1 - \frac{2m}{\beta r}\right)^{\frac{1-\alpha^2}{1+\alpha^2}} \mathrm{d}t^2 + \left(1 - \frac{2m}{\beta r}\right)^{-\frac{1-\alpha^2}{1+\alpha^2}} \mathrm{d}r^2$$

$$+r^2\left(1 - \frac{2m}{\beta r}\right)^{\frac{2\alpha^2}{1+\alpha^2}}\left[\mathrm{d}\theta^2 + \sin^2\theta\,\mathrm{d}\psi^2\right], \tag{19}$$

and

$$e^{\varphi} = \left(1 - \frac{2m}{\beta r}\right)^{\frac{\alpha}{1+\alpha^2}}, \tag{20}$$

with

$$\beta = \frac{1-\alpha^2}{1+\alpha^2}. \tag{21}$$

There are three possible branches:

- $\alpha > 0$: which we shall name α_+.
- $\alpha < 0$: which we shall name α_-.
- $\alpha = 0$: which we shall name α_0, and which simply is the Schwarzschild solution.

In the Einstein frame, the metric solutions for the branches α_+ and α_- are the same, but it is not the case in the original frame, as we shall see in the next section.

As one can see in Eq. (20), the sign of α gives the direction of the monotonicity of φ. One therefore deduces that α_0 corresponds to sources that are such that $\delta(\sqrt{-\tilde{g}}f)/\delta\varphi = 0$, α_+ corresponds to sources that are such that $\delta(\sqrt{-\tilde{g}}f)/\delta\varphi > 0$ and α_- corresponds to sources that are such that $\delta(\sqrt{-\tilde{g}}f)/\delta\varphi < 0$.

6 Solutions in the original frame

Performing the inverse conformal transformation – $g_{\alpha\beta} = e^{4\zeta\varphi}\tilde{g}_{\alpha\beta}$, with $\phi = e^{-4\zeta\varphi}$ and $\zeta := 1/(2\sqrt{3})$ – in order to get the corresponding solutions for the action (6), one either gets the usual Schwarzschild solution as limit (when $\alpha = 0$), or the two limits that follow. With the metric given by

$$g_{\mu\nu}\mathrm{d}x^\mu\mathrm{d}x^\nu = -a\mathrm{d}t^2 + b\mathrm{d}\rho^2 + \rho^2\mathrm{d}\Omega^2, \tag{22}$$

where $\mathrm{d}\Omega^2 = \mathrm{d}\theta^2 + \sin^2\theta\,\mathrm{d}\psi^2$, one has

$$a = \left(1 - \frac{2m}{\beta r}\right)^{\frac{1-\alpha^2+4\zeta\alpha}{1+\alpha^2}}, \tag{23}$$

$$b = \left(\frac{\mathrm{d}\rho}{\mathrm{d}r}\right)^{-2}\left(1 - \frac{2m}{\beta r}\right)^{\frac{\alpha^2-1+4\zeta\alpha}{1+\alpha^2}}, \tag{24}$$

$$\rho = r\left(1 - \frac{2m}{\beta r}\right)^{\frac{\alpha^2+2\zeta\alpha}{1+\alpha^2}}, \tag{25}$$

$$\phi = \left(1 - \frac{2m}{\beta r}\right)^{-\frac{4\zeta\alpha}{1+\alpha^2}}. \tag{26}$$

One can see that in this frame, the metric are different for the branches α_+ and α_- – which correspond to $\alpha > 0$ and $\alpha < 0$ respectively.

7 Comparing to external numerical solutions

With the metric given by

$$g_{\mu\nu}\mathrm{d}x^\mu\mathrm{d}x^\nu = -a\mathrm{d}t^2 + b\mathrm{d}\rho^2 + \rho^2\mathrm{d}\Omega^2, \tag{27}$$

the Tolman-Oppenheimer-Volkoff (TOV) equations for the action (6) outside an object in the vacuum limit reduce to

$$\frac{\ddot{\phi}}{\dot{\phi}} = \frac{1}{2}\left[\frac{\dot{b}}{b} - \frac{\dot{a}}{a} - \frac{4}{\rho}\right] \tag{28}$$

$$\frac{\dot{b}}{b} = \frac{1-b}{\rho} - \frac{\xi}{2}\frac{\dot{a}}{a} \tag{29}$$

$$\frac{\dot{a}}{a} = \frac{b-1}{\rho}\left[1+\frac{\xi}{2}\right]^{-1} - 2\frac{\xi}{\rho}\left[1+\frac{\xi}{2}\right]^{-1} \tag{30}$$

where $\xi \equiv \rho\dot{\phi}/\phi$. After integrating Eq. (28), one ends up with

$$\dot{\phi} = \frac{C}{\rho^2}\sqrt{\frac{b}{a}} \tag{31}$$

with C a constant of integration. The sign of C – which is such that $sign(C) = -sign(\alpha)$ (see Eq. (26)) – completely determines the monotonicity of ϕ.

One can check that each of the three vacuum limits discussed in Sect. 6 is indeed solution to the equations (28–30). It means that the three solutions α_0, α_- and α_+ should match external numerical solutions of the TOV equations found in Arruga et al. [2].

Entangled relativity being parameter free, the three cases can nevertheless be shown to correspond to the three different types of on-shell matter Lagrangians that one may consider – that is, $\mathcal{L}_m = T$, $\mathcal{L}_m = -\rho$ or $\mathcal{L}_m = P$, given that they correspond to no-source, positive or negative sources[8] in the scalar-field equation respectively. [Depending on the type of matter composing the compact object, one may have any of these cases [2]]. In what follows, we shall show that it is indeed the case, although the three cases actually more generally depend on whether the source of the scalar field is null, positive or negative respectively – since the various cases are related to the monoticity of ϕ, as one can see from Eq. (31).

The numerical integration is based on our previous work [2], in which we assumed a basic polytropic equation of state $P = K\rho^\gamma$ for simplicity, with $\gamma = 5/3$ and $K = 1.475 \times 10^{-3}(fm^3/MeV)^{2/3}$.

The code that does the numerical integration and generates all the figure of this manuscript is freely available on GitHub [1].

7.1 Comparison of α_0

It was found in Arruga et al. [2] that for $\mathcal{L}_m = T$ the TOV solutions in entangled relativity are the same as the ones of general relativity. It means that for $\mathcal{L}_m = T$, the external vacuum limit solution of compact objects is the Schwarzschild metric. Therefore, the case α_0 corresponds to compact objects that are made of matter that satisfy $\mathcal{L}_m = T$. Indeed, the extra degree of freedom of entangled relativity with respect to general relativity is not sourced in that case. Whether or not matter can lead to $\mathcal{L}_m = T$ is an ongoing debate [2–4].

In any case, as already discussed in Sect. 4, due the radiation of scalar hair during the collapse into a black hole in scalar–tensor theories [16,38], one expects that the Schwarzschild metric corresponds to black hole solutions, whether or not the Schwarzschild solution also corresponded to the external solution of the initial spherical compact object.

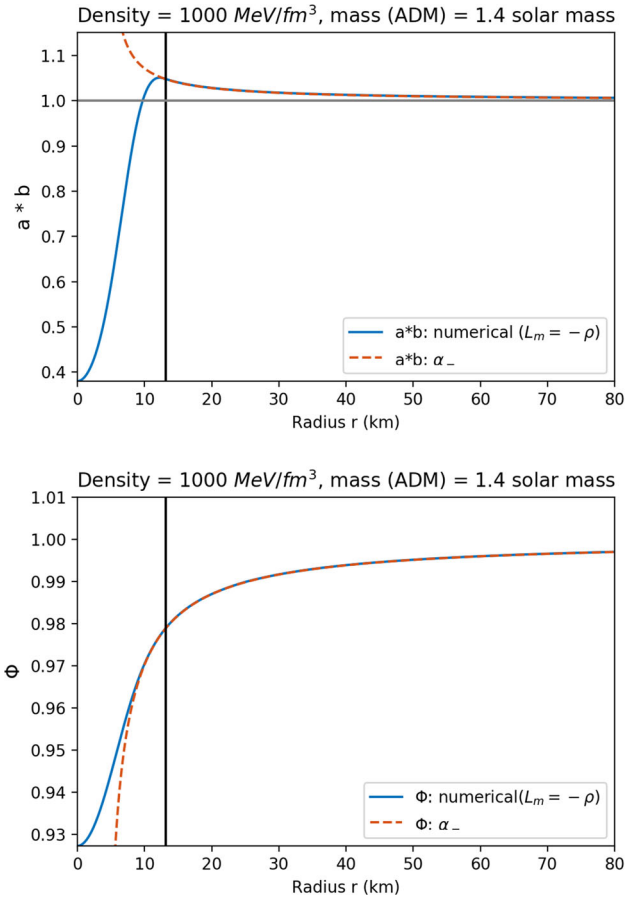

Fig. 1 Comparison of the product of the metric components and the scalar field between the analytical solution α_- and the numerical solution for $\mathcal{L}_m = -\rho$, and $\rho_0 = 1000\ MeV/fm^3$. The vertical line indicates the radius of the compact object

7.2 Comparison of α_-

The α_- case can be matched to the external part of the numerical TOV solutions for compact objects that are made of matter fields that satisfy $\mathcal{L}_m = -\rho$ – as one can see in Figs. 1 and 2.

[8] The source of the scalar-field equation is proportional to $\mathcal{L}_m - T$ in Eq. (10), such that it is null, positive or negative for $\mathcal{L}_m = T$, $\mathcal{L}_m = -\rho$ or $\mathcal{L}_m = P$ respectively. The corresponding value of C will therefore be null, positive or negative respectively, such that the corresponding value of α will be null, negative or positive respectively.

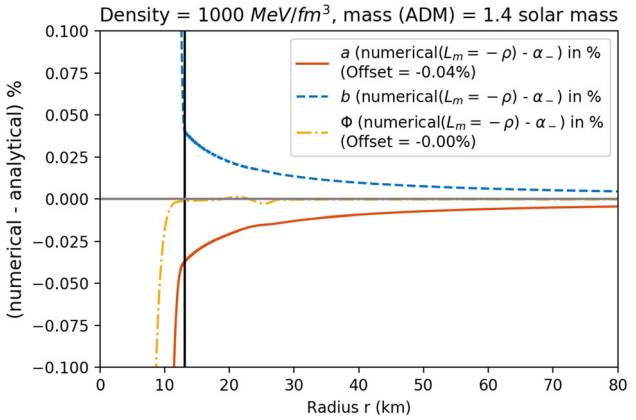

Fig. 2 % difference of the metric components and the scalar field between the analytical solution α_- and the numerical solution for $\mathcal{L}_m = -\rho$, for $\rho_0 = 1000\ MeV/fm^3$. The vertical line indicates the radius of the compact object

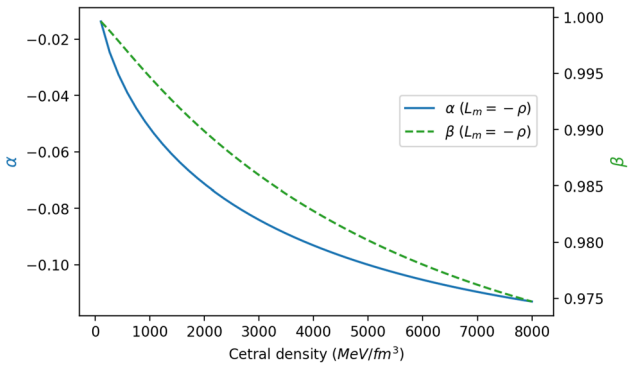

Fig. 3 Values of the parameters α and β in Eqs. (23–26) with respect to the density of the compact object for $\mathcal{L}_m = -\rho$

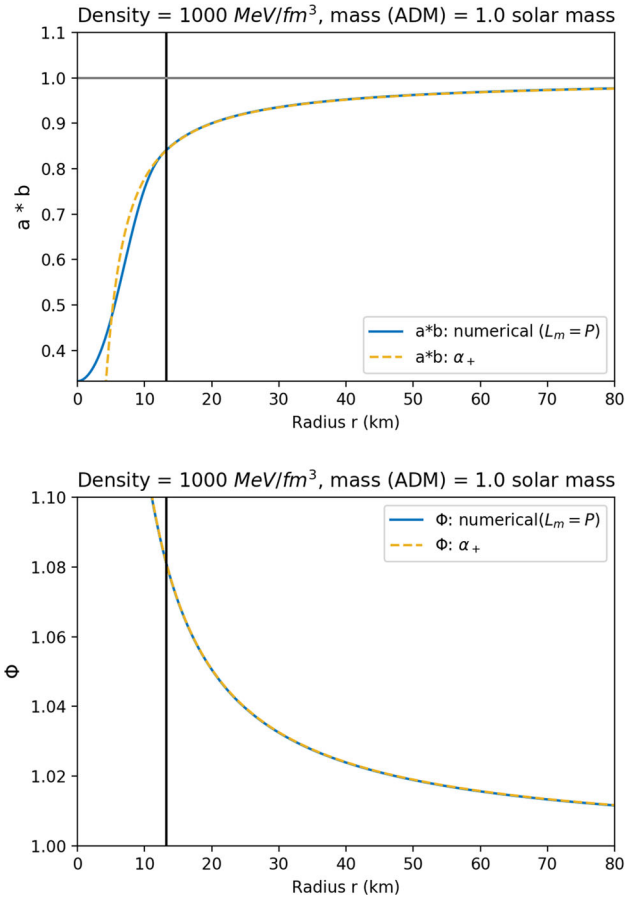

Fig. 4 Comparison of the product of the metric components and the scalar field between the analytical solution α_+ and the numerical solution for $\mathcal{L}_m = P$, and $\rho_0 = 1000\ MeV/fm^3$. The vertical line indicates the radius of the compact object

In particular, one can see the good agreement between the analytical and external numerical solutions in Fig. 2. Only a sub-permil deviation between the two solutions occurs at the limit of the compact object, and then decreases with the distance to the object. A sub-permil offset – which has been removed in Fig. 2 – remains for the time-time component of the metric a. It is easily explained by the fact that at the numerical level, one cannot use a normalization at infinity, but only at the limit of the simulation – that is, in our case, at $r = r_\infty := 10{,}000$ km.

One can see in Fig. 3 that there is a monotonic behavior of the parameters α and β in (23–26) with respect to the central density. For objects with low central densities, the solution is closer to the Schwarzschild solution – that is α is closer to 0, and β is closer to 1 – whereas the stronger the central density, the more the solution deviates from the Schwarzschild solution of general relativity. In other words, the more relativistic the object, the more deviation there is from general relativity.

More generally, the α_- case corresponds to spherical solutions for which the source of the scalar-field (i.e. r.h.s. of Eq. (10)) is positive.

7.3 Comparison of α_+

The α_+ case can be matched to numerical TOV solutions for compact objects that are made of matter that satisfy $\mathcal{L}_m = P$ – as one can see in Figs. 4 and 5. Although note that $\mathcal{L}_m = P$ is not consistent with a collection of baryonic particles, which Lagrangian must tend to $\mathcal{L}_m = -\rho_0$ for $P = 0$, where ρ_0 is the inertial energy density of the collection of particles. $\mathcal{L}_m = P$ might be used, however, in order to model exotic objects that would, for instance, entirely be made of a scalar field – given that $P = K - V = \mathcal{L}_m$ for scalar fields, where K and V are the kinetic and potential energy densities respectively. One may have in mind Higgs monopoles for instance, like in Schlögel et al. [39].

In particular, one can see the good agreement between the analytical and external numerical solutions in Fig. 5. Again,

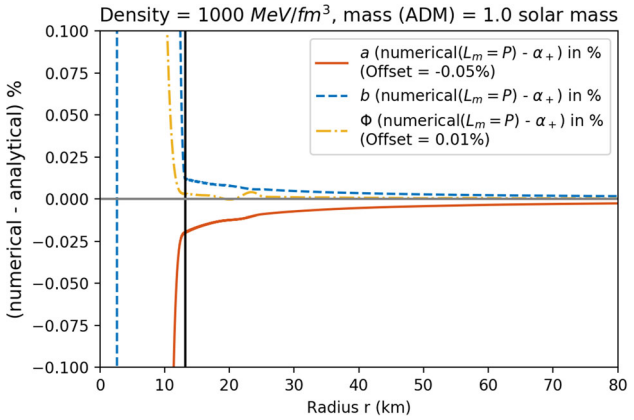

Fig. 5 % difference of the metric components and the scalar field between the analytical solution α_+ and the numerical solution for $\mathcal{L}_m = P$, for $\rho_0 = 1000\ MeV/fm^3$. The vertical line indicates the radius of the compact object

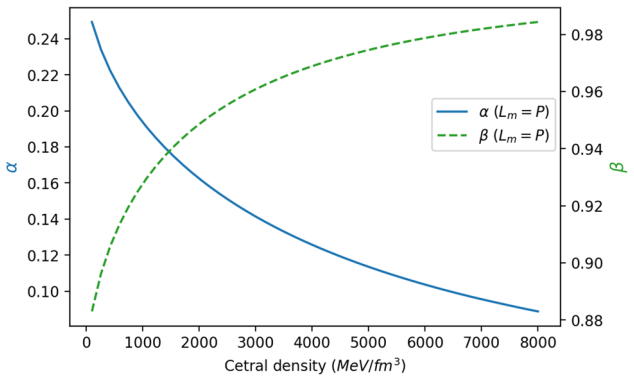

Fig. 6 Values of the parameters α and β in Eqs. (23–26) with respect to the density of the compact object for $\mathcal{L}_m = P$

a sub-permil deviation between the two solutions occurs at the limit of the compact object, and then decreases with the distance to the object. Again, a sub-permil offset remains for the time-time component of the metric (a).

As one can see in Fig. 6 the behavior of the parameters α and β in (23–26) is slightly different for α_+. Indeed, the more dense the compact object, the more close the Schwarzschild metric it becomes. [We have checked that this behavior reverses for much lower central densities – that is, that β goes back to one for much less dense objects]. Note that, given one has $\mathcal{L}_m = P > 0$, Eq. (8) implies that $R < 0$ for the α_+ case. We have checked that it is indeed the case in our TOV simulation.

More generally, the α_+ case corresponds to spherical solutions for which the source of the scalar-field (i.e. r.h.s. of Eq. (10)) is negative.

8 Test particle geodesics

We assume that the action (6) induces for test particles that their action reads $S_{\rm tp} = -mc^2 \int \sqrt{\phi} d\tau$, where τ is an affine parameter of the test particle's trajectory defined such that $d\tau = \sqrt{-g_{\alpha\beta} dx^\alpha dx^\beta}$. This assumption follows the assumption of the stability of the universal coupling at the quantum field theory level, such that all the contributions to the mass of a particle are proportional to the same function of the scalar field ϕ, which can therefore be factorized out as $m(\phi) \to \sqrt{\phi}\, m$. In particular, it means that we assume that

$$\sqrt{\phi}\mathcal{L}_m^{SM} \to \sqrt{\phi} T^{\rm SM}_{\rm anomaly}, \tag{32}$$

where $\mathcal{L}_m^{SM}$ is the effective low energy limit of the standard model of particles and $T^{\rm SM}_{\rm anomaly}$ its corresponding quantum trace anomaly [30,34] – which gives their mass to composite particles in the standard model of particles [9].

After the conformal transformation $\tilde{g}_{\alpha\beta} = e^{-2\varphi/\sqrt{3}} g_{\alpha\beta}$, with $\phi = e^{-2\varphi/\sqrt{3}}$, defined in Sect. 5, the test particle part of the action reads $S_{\rm tp} = -mc^2 \int d\tilde{\tau}$, where $d\tilde{\tau} = \sqrt{-\tilde{g}_{\alpha\beta} dx^\alpha dx^\beta}$. The whole action with a neutral massive test particle in the conformal frame therefore reads

$$S = \int d^4x \sqrt{-\tilde{g}} \left[\tilde{R} - 2(\tilde{g}^{\alpha\beta} \partial_\alpha \varphi \partial_\beta \varphi) - e^{-\varphi/\sqrt{3}} \frac{\tilde{F}^2}{4} \right] - mc^2 \int d\tilde{\tau}, \tag{33}$$

where $\sqrt{-\tilde{g}} \tilde{F}^2 = \sqrt{-g} F^2 := \sqrt{-g} F_{\alpha\beta} F^{\alpha\beta}$ due to the conformal invariance of the electromagnetic part of the action at the classical level, with $F_{\alpha\beta} = \nabla_\alpha A_\beta - \nabla_\beta A_\alpha$, and A^α the electromagnetic four-vector.

The electromagnetic contribution to the mass m (through the trace anomaly in Eq. (32)), by definition, breaks the conformal invariance of the electromagnetic part of the action (6), leading to the universal effective coupling $S_{\rm tp} = -mc^2 \int \sqrt{\phi} d\tau$ in the original frame (6) – which effectively corresponds to having a mass that is proportional to $\sqrt{\phi}$. This is why m can become independent of the scalar-field in the Einstein frame. It is important to stress that – except for the special case of general relativity – it would not be the case (at least, in general) for other functions $f(\varphi, \tilde{\mathcal{L}}_m)$ than the one of entangled relativity, given in Eq. (18). This shows how, despite its very unusual form in Eq. (1), entangled relativity actually is pretty close to general relativity, as one can see in Eq. (33). Only a coupling of an effective scalar degree of freedom to the electromagnetic part of the action remains in the Einstein frame for neutral point particles.

Therefore, neutral massive test particles follow geodesics of the conformal metric $\tilde{g}_{\alpha\beta}$. However, it is important to stress that the affine parameter on the geodesic $\tilde{\tau}$ is not the time

given by, say, an atomic clock along the geodesics, since the latter depends on the variation of the fine structure constant that should be proportional to $e^{\varphi/\sqrt{3}}$ in this model [17,29]. Entangled relativity therefore seems to break the *local position invariance* in general – that is, as long as φ is not constant. Fortunately enough, the embedded *intrinsic decoupling* in entangled relativity implies a near constant scalar field in most situations [2,24,26,28,29,31].

One can show that electromagnetic plane-waves in the geometric optic approximation also follow null-geodesics of either the metric $g_{\alpha\beta}$ or its conformally transformed version $\tilde{g}_{\alpha\beta}$ [29]. This is due to the conformal invariance of the electromagnetic part of the action at the classical level.

Working in the plane $\theta = \pi/2$ without loss of generality, one deduces the following equations of motion from Eq. (13)

$$\left(\frac{\mathrm{d}r}{\mathrm{d}\tilde{\tau}}\right)^2 + \tilde{\lambda}^2(r)\left[\epsilon + \frac{L^2}{\tilde{\rho}^2(r)}\right] = E^2, \tag{34}$$

$$\tilde{\rho}^2(r)\frac{\mathrm{d}\psi}{\mathrm{d}\tilde{\tau}} = L, \tag{35}$$

$$\tilde{\lambda}^2(r)\frac{\mathrm{d}t}{\mathrm{d}\tilde{\tau}} = E, \tag{36}$$

where

$$\tilde{\rho}^2(r) = r^2\left(1 - \frac{2m}{\beta r}\right)^{1-\beta}, \tag{37}$$

$$\tilde{\lambda}^2(r) = \left(1 - \frac{2m}{\beta r}\right)^{\beta}. \tag{38}$$

and where E and L are the conserved energy and momentum along the trajectories respectively, and where ϵ is either equal to 0 or 1 for null and time-like geodesics respectively.

One can define an effective radial potential that reads

$$V_{\mathrm{eff}}(r) = \frac{1}{2}\left(-E^2 + \tilde{l}^2(r)\frac{L^2}{r^2} + \tilde{\lambda}^2(r)\epsilon\right), \tag{39}$$

where

$$\tilde{l}^2(r) := \left(1 - \frac{2m}{\beta r}\right)^{2\beta-1}. \tag{40}$$

We have plotted some examples of null and timelike geodesics in Fig. 7.

8.1 Shapiro delay

The electromagnetic Lagrangian density being conformally invariant at the classical level, one can compute the Shapiro delay from any metric related by a conformal transformation and get the same result. From Eq. (13), the relative time delay [42] from the surface of the spherical object $r = R > 2m/\beta$ therefore reads

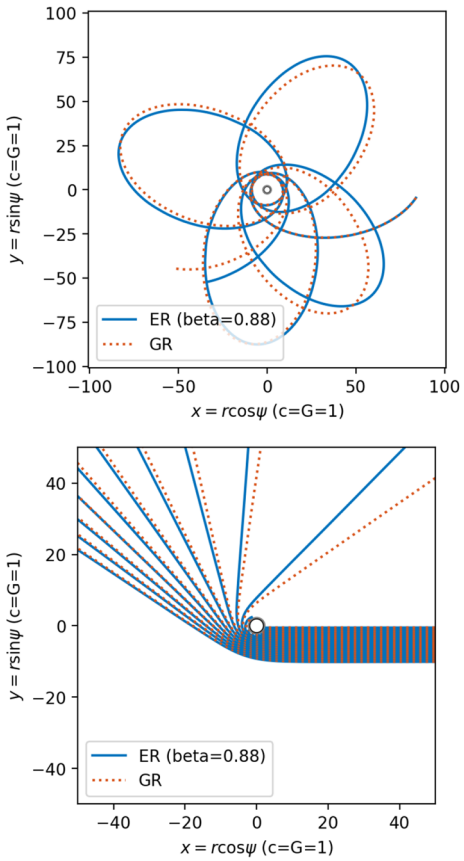

Fig. 7 Upper panel: timelike geodesics parametrized by the coordinate time t, with $m = 1$, $E = 0.98$, $L = 4.5$, for $\beta = 1$ (general relativity) versus $\beta = 0.88$, which corresponds to the lowest value found in our TOV simulations in entangled relativity, for an exotic compact object (i.e. $\mathcal{L}_m = P$) – see Fig. 6. Note that for a more realistic object (i.e. $\mathcal{L}_m = -\rho$ or T), the lowest value has been found to be $\beta = 0.975$ instead – see Fig 3. Lower panel: null geodesics parametrized by the coordinate time t with various impact parameters, with $m = 1$, for $\beta = 1$ (general relativity) versus $\beta = 0.88$

$$\delta t(\sigma) = \int_R^\infty \frac{1}{\tilde{\lambda}^2(r)}\left(\frac{1}{\sqrt{1 - \frac{\sigma^2\tilde{l}^2(r)}{r^2}}} - 1\right)\mathrm{d}r \tag{41}$$

where the impact parameter σ satisfies $\sigma = L/E$, while $\tilde{\lambda}(r)$ and $\tilde{l}(r)$ are given in Eqs. (38) and (40) respectively.

$\delta t(\sigma)$ is the traveling time $t(\sigma) - t$, minus the reception time of an hypothetical radial ray $t(\sigma = 0)$. It is simply meant to define a usefull finite quantity after an integration over infinity, which can also be used to relate the emission and reception times in terms of the periodic change of the impact parameter of the hot spots at the surface of the neutron star [42].

9 Conclusion

In this manuscript, we provided external analytical solutions for spherical objects valid for a very general class of scalar–tensor theories. From them, we derived the specific external analytical solutions for spherical objects in entangled relativity, which we compared to numerical solutions. We found that analytical and numerical solutions match very well outside the compact objects – therefore providing evidence that both types of solutions are valid.

A direct use of these simple analytical solutions would be to use them instead of the more complex numerical solutions in order to infer, say, a neutron star's mass, radius and scalar hair. Indeed, whereas numerical solutions rely on the unknown equation of state of neutron stars, analytical solutions are parametrized by only two parameters – that is, the mass and a parameter related to the amplitude of the scalar hair. It therefore greatly simplifies the model to be adjusted to observations.

We also provided the relevant equations in order to compute such observables.

Acknowledgements O.M. acknowledges support from the *Fondation des frères Louis et Max Principale*. The authors thank Alessandro Roussel – owner of the YouTube channel ScienceClic [37] – for simulating the gravitational lens from the metric in Eq. (13), and for understanding that two metrics with a same values for m and $|\beta|$ were actually the same metric – see Sect. Appendix C.

Data Availability Statement This manuscript has no associated data or the data will not be deposited. [Authors' comment: No data were used in this work.]

Funded by SCOAP[3].

Appendix A: General metric field equation of entangled relativity

The metric field equation that derives from the action (1), reads ($\forall \mathcal{L}_m$)

$$\frac{\mathcal{L}_m^2}{R^2}\left(R_{\mu\nu}-\frac{1}{2}g_{\mu\nu}R\right) = -\frac{\mathcal{L}_m}{R}T_{\mu\nu} + \left(\nabla_\mu\nabla_\nu - g_{\mu\nu}\Box\right)\frac{\mathcal{L}_m^2}{R^2}. \tag{A.1}$$

Therefore, for $\mathcal{L}_m \neq 0$, Eq. (A.1) can indeed be rewritten as Eq. (2).

If the on-shell matter Lagrangian goes to zero during a transition between $\mathcal{L}_m > 0$ and $\mathcal{L}_m < 0$ whereas $R \neq 0$, the field equation at the location of the transition reduces to $\left(\nabla_\mu\nabla_\nu - g_{\mu\nu}\Box\right)\mathcal{L}_m^2/R^2 = 0$.

Appendix B: Check external analytical solution

– From the action in Eq. (11), the metric field equation at the vacuum limit reads

$$G_{\alpha\beta} = 2\left[\partial_\alpha\varphi\partial_\beta\varphi - \frac{1}{2}g_{\alpha\beta}(\partial\varphi)^2\right] =: S_{\alpha\beta}, \tag{B.2}$$

where $G_{\alpha\beta}$ is the usual Einstein tensor. From the metric in Eq. (13), one gets the following non-null mixed components of the Einstein tensor

$$G_0^0 = \frac{\beta^2-1}{\beta^2}\frac{m^2}{r^4}\left(1-\frac{2m}{\beta r}\right)^{\beta-2} = G_\theta^\theta = G_\psi^\psi = -G_r^r, \tag{B.3}$$

whereas the non-null mixed components of the source reads

$$S_0^0 = -g^{rr}\left(\frac{\partial\varphi}{\partial r}\right)^2 = S_\theta^\theta = S_\psi^\psi = -S_r^r. \tag{B.4}$$

One finds that $G_0^0 = S_0^0$, such that one has checked that $G_{\alpha\beta} = S_{\alpha\beta}$.

– From the action in Eq. (11), the scalar field equation at the vacuum limit reads

$$\Box\varphi = g^{rr}\varphi'' - g^{\alpha\beta}\Gamma^r_{\alpha\beta}\varphi' = 0. \tag{B.5}$$

From the mertic (13) and the scalar field (14) equations, one gets

$$g^{\alpha\beta}\Gamma^r_{\alpha\beta}\varphi' = \frac{\beta-1}{\alpha}\frac{2m^2}{r^4}\left(1-\frac{2m}{\beta r}\right)^{\beta-2}\left(\frac{m\beta-r}{m\beta}\right),$$

(B.6)

such that one can check that

$$g^{rr}\varphi'' = g^{\alpha\beta}\Gamma^{r}_{\alpha\beta}\varphi'. \tag{B.7}$$

Therefore, one indeed has verified that $\Box\varphi = 0$.

Appendix C: Mapping between the β and $-\beta$ solutions

Defining $\rho = r - 2m/\beta$, one gets

$$1 - \frac{2m}{\beta r} = \left(1 + \frac{2m}{\beta\rho}\right)^{-1}, \tag{C.8}$$

such that the Eqs. (13–14) read

$$ds^2 = -\left(1 + \frac{2m}{\beta\rho}\right)^{-\beta} \mathrm{d}t^2 + \left(1 + \frac{2m}{\beta\rho}\right)^{\beta} \mathrm{d}\rho^2 + \rho^2 \left(1 + \frac{2m}{\beta\rho}\right)^{1+\beta} \left[\mathrm{d}\theta^2 + \sin^2\theta\, \mathrm{d}\psi^2\right], \tag{C.9}$$

that is, it is Eq. (13) with $\beta \to -\beta$ when $r \to \rho$. In particular, one can see that the metric in Eq. (13) with $\beta = -1$ corresponds to the exterior of the Schwarzschild solution – that is, $\beta = 1$ in Eq. (13) – because ρ goes from the event horizon $r = 2m$ to infinity. Otherwise, the scalar field transforms as

$$\varphi = \frac{\beta - 1}{2\alpha} \ln\left(1 + \frac{2m}{\beta\rho}\right). \tag{C.10}$$

Appendix D: Curvature singularity

The Ricci scalar of the metric in Eq. (13) reads

$$R = -2\frac{\beta^2 - 1}{\beta^2}\frac{m^2}{r^4}\frac{1}{\left(1 - \frac{2m}{\beta r}\right)^{2-\beta}}, \tag{D.11}$$

such that one can check that it diverges at $r = 2m/\beta\ \forall\ \beta \in]0; 1[$. $r = 2m/\beta$ therefore is a curvature singularity for all $\beta \in]0; 1[$. For $\beta \in]-1; 0[$, the Ricci scalar only diverges at $r = 0$. The reason simply being that the metric with $\beta < 0$ correspond to the metric with $\beta > 0$ with a shifted radial coordinate $r \to r + 2m/\beta$. See Sect. Appendix C. For $|\beta| < 1$, the Ricci scalar is positive, whereas one recovers the flatness of the Schwarzschild metric – that is $R = 0$ – for $|\beta| = 1$.

References

1. D. Arruga, O. Minazzoli, Code and script to compute all the figures. https://github.com/denisArruga/TOVversusAnalytical
2. D. Arruga, O. Rousselle, O. Minazzoli, Compact objects in entangled relativity. Phys. Rev. D **103**(2), 024034 (2021). https://doi.org/10.1103/PhysRevD.103.024034
3. P.P. Avelino, R.P.L. Azevedo, Perfect fluid Lagrangian and its cosmological implications in theories of gravity with nonminimally coupled matter fields. Phys. Rev. D **97**(6), 064018 (2018). https://doi.org/10.1103/PhysRevD.97.064018
4. P.P. Avelino, L. Sousa, Matter Lagrangian of particles and fluids. Phys. Rev. D **97**(6), 064019 (2018). https://doi.org/10.1103/PhysRevD.97.064019
5. E. Berti, E. Barausse, V. Cardoso, L. Gualtieri, P. Pani, U. Sperhake, L.C. Stein, N. Wex, K. Yagi, T. Baker, C.P. Burgess, F.S. Coelho, D. Doneva, A. De Felice, P.G. Ferreira, P.C.C. Freire, J. Healy, C. Herdeiro, M. Horbatsch, B. Kleihaus, A. Klein, K. Kokkotas, J. Kunz, P. Laguna, R.N. Lang, T.G.F. Li, T. Littenberg, A. Matas, S. Mirshekari, H. Okawa, E. Radu, R. O'Shaughnessy, B.S. Sathyaprakash, C. Van Den Broeck, H.A. Winther, H. Witek, M.E. Aghili, J. Alsing, B. Bolen, L. Bombelli, S. Caudill, L. Chen, J.C. Degollado, R. Fujita, C. Gao, D. Gerosa, S. Kamali, H.O. Silva, J.G. Rosa, L. Sadeghian, M. Sampaio, H. Sotani, M. Zilhao, Testing general relativity with present and future astrophysical observations. Class. Quantum Gravity **32**(24), 243001 (2015). https://doi.org/10.1088/0264-9381/32/24/243001
6. S. Bogdanov, F.K. Lamb, S. Mahmoodifar, M.C. Miller, S.M. Morsink, T.E. Riley, T.E. Strohmayer, A.K. Tung, A.L. Watts, A.J. Dittmann, D. Chakrabarty, S. Guillot, Z. Arzoumanian, K.C. Gendreau, Constraining the neutron star mass-radius relation and dense matter equation of state with NICER. II. Emission from hot spots on a rapidly rotating neutron star. Astrophys. Lett. **887**(1), L26 (2019). https://doi.org/10.3847/2041-8213/ab5968
7. T. Damour, G. Esposito-Farese, Tensor-multi-scalar theories of gravitation. Class. Quantum Gravity **9**(9), 2093–2176 (1992). https://doi.org/10.1088/0264-9381/9/9/015
8. T. Damour, A.M. Polyakov, The string dilation and a least coupling principle. Nucl. Phys. B **423**(2–3), 532–558 (1994). https://doi.org/10.1016/0550-3213(94)90143-0
9. F.J. Donoghue, E. Golowich, R. Barry, *Holstein. Dynamics of the Standard Model* (Cambridge University Press, Cambridge, 2014)
10. A. Einstein, Prinzipielles zur allgemeinen Relativitätstheorie. Annalen der Physik **360**(4), 241–244 (1918). https://doi.org/10.1002/andp.19183600402
11. Event Horizon Telescope Collaboration, First M87 Event Horizon Telescope Results. I. The Shadow of the Supermassive Black Hole. Astrophys. Lett. 875(1), L1 (2019). https://doi.org/10.3847/2041-8213/ab0ec7
12. D. Garfinkle, G.T. Horowitz, A. Strominger, Charged black holes in string theory. Phys. Rev. D **43**(10), 3140–3143 (1991). https://doi.org/10.1103/PhysRevD.43.3140
13. G.W. Gibbons, K.-I. Maeda, Black holes and membranes in higher-dimensional theories with dilaton fields. Nucl. Phys. B **298**(4), 741–775 (1988). https://doi.org/10.1016/0550-3213(88)90006-5
14. A.A.H. Graham, R. Jha, Stationary black holes with time-dependent scalar fields. Phys. Rev. D **90**(4), 041501 (2014). https://doi.org/10.1103/PhysRevD.90.041501
15. J.B. Griffiths, J. Podolský, *Exact Space-Times in Einstein's General Relativity* (Cambridge University Press, Cambridge, 2012)
16. S.W. Hawking, Black holes in the Brans–Dicke: theory of gravitation. Commun. Math. Phys. **25**(2), 167–171 (1972). https://doi.org/10.1007/BF01877518
17. A. Hees, O. Minazzoli, J. Larena, Breaking of the equivalence principle in the electromagnetic sector and its cosmological sig-

natures. Phys. Rev. D **90**(12), 124064 (2014). https://doi.org/10.1103/PhysRevD.90.124064
18. C.F.E. Holzhey, F. Wilczek, Black holes as elementary particles. Nucl. Phys. B **380**(3), 447–477 (1992). https://doi.org/10.1016/0550-3213(92)90254-9
19. A.I. Janis, E.T. Newman, J. Winicour, Reality of the Schwarzschild singularity. Phys. Rev. Lett. **20**(16), 878–880 (1968). https://doi.org/10.1103/PhysRevLett.20.878
20. M.D. Johnson, A. Lupsasca, A. Strominger, G.N. Wong, S. Hadar, D. Kapec, R. Narayan, A. Chael, C.F. Gammie, P. Galison, D.C.M. Palumbo, S.S. Doeleman, L. Blackburn, M. Wielgus, D.W. Pesce, J.R. Farah, J.M. Moran, Universal interferometric signatures of a black hole's photon ring. Sci. Adv. **6**(12), eaaz1310 (2020). https://doi.org/10.1126/sciadv.aaz1310
21. K. Just, Notizen: the motion of mercury according to the theory of Thiry and Lichnerowicz. Zeitschrift Naturforschung Teil A **14**(8), 751 (1959). https://doi.org/10.1515/zna-1959-0810
22. H. Ludwig, O. Minazzoli, S. Capozziello, Merging matter and geometry in the same Lagrangian. Phys. Lett. B **751**, 576–578 (2015). https://doi.org/10.1016/j.physletb.2015.11.023
23. M.C. Miller, F.K. Lamb, A.J. Dittmann, S. Bogdanov, Z. Arzoumanian, K.C. Gendreau, S. Guillot, A.K. Harding, W.C.G. Ho, J.M. Lattimer, R.M. Ludlam, S. Mahmoodifar, S.M. Morsink, P.S. Ray, T.E. Strohmayer, K.S. Wood, T. Enoto, R. Foster, T. Okajima, G. Prigozhin, Y. Soong, PSR J0030+0451 mass and radius from NICER data and implications for the properties of neutron star matter. Astrophys. Lett. **887**(1), L24 (2019). https://doi.org/10.3847/2041-8213/ab50c5
24. O. Minazzoli, On the cosmic convergence mechanism of the massless dilaton. Phys. Lett. B **735**, 119–121 (2014). https://doi.org/10.1016/j.physletb.2014.06.027
25. O. Minazzoli, Rethinking the link between matter and geometry. Phys. Rev. D **98**(12), 124020 (2018). https://doi.org/10.1103/PhysRevD.98.124020
26. O. Minazzoli, De Sitter space-times in Entangled Relativity. (2020) arXiv e-prints, art. arXiv:2011.14633
27. O. Minazzoli, Spacetime might not be doomed after all. (2021) arXiv e-prints, art. arXiv:2103.05313
28. O. Minazzoli, A. Hees, Intrinsic solar system decoupling of a scalar–tensor theory with a universal coupling between the scalar field and the matter Lagrangian. Phys. Rev. D **88**(4), 041504 (2013). https://doi.org/10.1103/PhysRevD.88.041504
29. O. Minazzoli, A. Hees, Late-time cosmology of a scalar–tensor theory with a universal multiplicative coupling between the scalar field and the matter Lagrangian. Phys. Rev. D **90**(2), 023017 (2014). https://doi.org/10.1103/PhysRevD.90.023017
30. O. Minazzoli, A. Hees, Dilatons with intrinsic decouplings. Phys. Rev. D **94**(6), 064038 (2016). https://doi.org/10.1103/PhysRevD.94.064038
31. O. Minazzoli, E. Santos, Charged black hole and radiating solutions in entangled relativity. (2021) arXiv e-prints, art. arXiv:2102.10541
32. O. Minazzoli, E. Santos, Charged black hole and radiating solutions in entangled relativity. (2021) arXiv e-prints, art. arXiv:2102.10541
33. Y. Mizuno, Z. Younsi, C.M. Fromm, O. Porth, M. De Laurentis, H. Olivares, H. Falcke, M. Kramer, L. Rezzolla, The current ability to test theories of gravity with black hole shadows. Nat. Astron. **2**, 585–590 (2018). https://doi.org/10.1038/s41550-018-0449-5
34. F. Nitti, F. Piazza, Scalar–tensor theories, trace anomalies, and the QCD frame. Phys. Rev. D **86**(12), 122002 (2012). https://doi.org/10.1103/PhysRevD.86.122002
35. A. Pais, *Subtle Is the Lord. The Science and the Life of Albert Einstein* (Oxford University Press, Oxford, 1982)
36. T.E. Riley, A.L. Watts, S. Bogdanov, P.S. Ray, R.M. Ludlam, S. Guillot, Z. Arzoumanian, C.L. Baker, A.V. Bilous, D. Chakrabarty, K.C. Gendreau, A.K. Harding, W.C.G. Ho, J.M. Lattimer, S.M. Morsink, T.E. Strohmayer, A NICER View of PSR J0030+0451: millisecond pulsar parameter estimation. Astrophys. Lett. **887**(1), L21 (2019). https://doi.org/10.3847/2041-8213/ab481c
37. A. Roussel, Scienceclic: YouTube channel of Alessandro Roussel. https://www.youtube.com/channel/UCWvq4kcdNI1r1jZKFw9TiUA
38. M.A. Scheel, S.L. Shapiro, S.A. Teukolsky, Collapse to black holes in Brans–Dicke theory. II. Comparison with general relativity. Phys. Rev. D **51**(8), 4236–4249 (1995). https://doi.org/10.1103/PhysRevD.51.4236
39. S. Schlögel, M. Rinaldi, F. Staelens, A. Füzfa, Particle like solutions in modified gravity: the Higgs monopole. Phys. Rev. D **90**(4), 044056 (2014). https://doi.org/10.1103/PhysRevD.90.044056
40. T.P. Sotiriou, V. Faraoni, Black holes in scalar–tensor gravity. Phys. Rev. Lett. **108**(8), 081103 (2012). https://doi.org/10.1103/PhysRevLett.108.081103
41. C.M. Will, The confrontation between general relativity and experiment. Living Rev. Relativ. **17**(1), 4 (2014). https://doi.org/10.12942/lrr-2014-4
42. R. Xu, Y. Gao, L. Shao, Strong-field effects in massive scalar–tensor gravity for slowly spinning neutron stars and application to X-ray pulsar pulse profiles. Phys. Rev. D **102**(6), 064057 (2020). https://doi.org/10.1103/PhysRevD.102.064057